Optical Engineering

OpticalEngineering.SPIEDigitalLibrary.org

Large angle nonmechanical laser beam steering at 4.6 μm using a digital micromirror device

James Ryan Lindle
Abbie T. Watnik

SPIE.

James Ryan Lindle, Abbie T. Watnik, "Large angle nonmechanical laser beam steering at 4.6 μm using a digital micromirror device," *Opt. Eng.* **57**(2), 027108 (2018), doi: 10.1117/1.OE.57.2.027108.

Large angle nonmechanical laser beam steering at 4.6 μm using a digital micromirror device

James Ryan Lindle* **and Abbie T. Watnik**
U.S. Naval Research Laboratory, Washington, DC, United States

Abstract. Large angle, nonmechanical beam steering is demonstrated at 4.62 μm using the digital light processing technology. A 42-deg steering range is demonstrated, limited by the field-of-view of the recollimating lens. The measured diffraction efficiency is 8.1% on-axis and falls-off with a $\sin^2$ dependence with the steering angle. However, within the 42-deg steering range, the power varied less than 25%. The profile of the steered laser beam is Gaussian with a divergence of 5.2 mrad. Multibeam, randomly addressable beam steering, is also demonstrated. [DOI: 10.1117/1.OE.57.2.027108]

Keywords: nonmechanical beam steering; spatial light modulators; digital micromirror devices.

Paper 171699 received Oct. 26, 2017; accepted for publication Jan. 30, 2018; published online Feb. 27, 2018.

1 Introduction

Over the past few years, the development of smaller, lighter beam steering devices with low power requirements has come to the forefront in response to applications such as remote LIDAR systems for chemical sensing as well as for reconnaissance, surveillance, and navigational systems for robots, drones, autonomous vehicles, and autonomous ships.[1–6] Other applications include communications systems, laser designators, and countermeasure systems against missile attacks. Several nonmechanical beam steering technologies have been demonstrated in the visible, near-infrared (NIR), and short wave IR (SWIR) spectral regions including systems based on diffraction [such as spatial light modulators (SLM),[7] optical phased arrays,[8] and polarization gratings[9]] and refraction (for example, the SEEOR technology[10] or tunable liquid lenses[1]). However, there have only been a few beam steering research programs dedicated to the midwave IR (MWIR, 3 to 5 μm) spectral region, a critical spectral region for chemical sensing and laser countermeasures, and most of them have investigated mechanical devices.

Currently, mechanical devices are used to steer laser beams in the MWIR spectral region. Most of these systems use gimbal-mounted mirrors,[11] although a number of applications implement rotating Risley prisms.[12] These steering systems require significant maintenance, have mechanical failure issues, and their speed is limited by the inertia of the optical component. Moreover, these mechanical systems do not meet the size, weight, and power (SWAP) requirements of small aerial platforms. On the other hand, nonmechanical systems do not suffer from the above mechanical or SWAP limitations, and since they are randomly addressable, not slewed, their speed is not limited by inertia but by the frame rate. Whereas the mechanical system can only address one target, the nonmechanical system can address multiple targets simultaneously[3] with a wavelength agile laser beam.[13] The wavelength, position, and intensity of each beam can be independently controlled. Each wavelength from a repertoire of copropagating lasers can be steered on target either simultaneously or sequentially. Furthermore, since the angular resolution of the discretely steered beam is less than the divergence of the laser beam (that is, the beam size is larger than the minimum angular step size), there is full coverage of the field of engagement.

Recently, nonmechanical MWIR beam steering was demonstrated in chalcogenide glass waveguides based on the SEEOR technology.[14] Two-dimensional beam steering of 2.74 degrees in plane and 0.3 deg out-of-plane was demonstrated at 4.6 μm. The out-of-plane steering angle could potentially be magnified at a fixed wavelength by a series of devices employing liquid crystal polarization gratings as demonstrated by Davis[6] in the SWIR spectral region. However, the MWIR polarization grating devices would need to be developed. In addition, the efficiency and speed of the device were not addressed in that paper.

In this paper, we will demonstrate large angle, nonmechanical beam steering at 4.6 μm using an SLM. In previous publications,[7,13] we demonstrated that a visible laser beam could be efficiently steered over a large field of engagement by rendering digital holographic patterns on a liquid crystal SLM. Unfortunately, at the present time, there are no commercially available MWIR liquid crystal SLMs capable of efficient large angle beam steering. (Meadowlark has sold several devices for IR scene projection; however, the phase delay of these devices is not sufficient for efficient beam steering). Also, it should be noted that as the wavelength increases, the thickness of the nematic liquid crystal layer required for a 2-pi phase delay increases and the time response increases as the square of the thickness;[15] that is, the speed of the liquid crystal device decreases nonlinearly with wavelength. Consequently, a digital micromirror device (DMD) is used in this research.

The DMD device that is used in this research was manufactured by Texas Instruments using the digital light processing technology (DLP). The DLP device was chosen, because it is a mature technology that has been used throughout the ultraviolet, visible, NIR and infrared spectral regions

*Address all correspondence to: James Ryan Lindle, E-mail: lindle@nrl.navy.mil

and it can operate at speeds exceeding 10 kHz. Several beam steering approaches have been used with the DLP technology including gratings,[16] subarrays,[17] and Fresnel zone plates (FZP).[18,19] In the grating approach, steering is accomplished by changing the grating spacing. Since the steering angle is inversely proportional to the grating spacing, steering at large angles (small grating spacing) results in coarse sampling. Some authors[20] have shown that finer steering can be obtained using intrapixel resets with a phase only SLM; however, the efficiency is severely reduced. Moreover, this technique is not applicable to a binary amplitude device and thus intrapixel steering will not be considered further here. The subarray approach activates a single mirror or a small area of mirrors that can be randomly addressed within the confines of the SLM. Addressing different mirrors is equivalent to steering the beam, since each mirror corresponds to a different location in the far field. However, if only one mirror is activated, the light illuminating the rest of the SLM will be discarded resulting in a very low power efficiency in the steered beam. In the FZP approach, steering is implemented by moving the position of the zone center (the phase pattern remains the same as the zone center is translated across the SLM), which is not confined to the physical area of the SLM. However, since the width of the zones decreases with the distance from zone center, there will be a position where the zone width becomes thinner than the SLM pixel pitch. At a wavelength of 4.6 μm and a focal length of 250 mm, this does not occur until the zone center is moved far off the physical dimensions of the SLM. In our experimental configuration, the beam hits the field stop of the recollimating lens before it reaches this limit. The angular resolution, corresponding to moving the zone center one pixel, is much higher at large angles when compared to the grating approach. In addition, the FZP approach provides a larger steering range and higher intensity than the subarray approach. Consequently, the FZP approach is used here.

2 Experimental Setup

The experimental setup is shown in Fig. 1. The output of a doubled carbon dioxide laser, operating at 4.6 μm, is chopped, spatially filtered and expanded (4×) to fill the aperture of the DLP. An iris is inserted into the beam to restrict the beam size to the active region of the DLP. The DLP is rotated 45 deg about the normal to the window such that the hinged diagonal of the DLP is vertical and perpendicular to the plane of the optical table top. The laser beam is incident on the DLP at 24 deg to the window normal, and the DLP is aligned so that the light reflected from a flat binary 1 pattern (nominally a 12-deg tilt) is at normal incident to the DLP window, designated as on-axis. A flat binary 0 pattern (−12-deg tilt) reflects the laser beam into a beam dump. An MWIR PbSe detector monitors the incident power. An FZP, a diffractive optical lens with a focal length of 250 mm, is rendered on the SLM that is configured as the first element of a telescope and steering is generated by moving the zone center of the FZP. The steering angle is magnified 5× by a 50-mm focal length, $f/1.2$ recollimating lens. An MWIR camera is used to observe the steered beam across a screen inserted into the beam path. The lens-to-screen distance is long compared to the focal length of the recollimating lens.

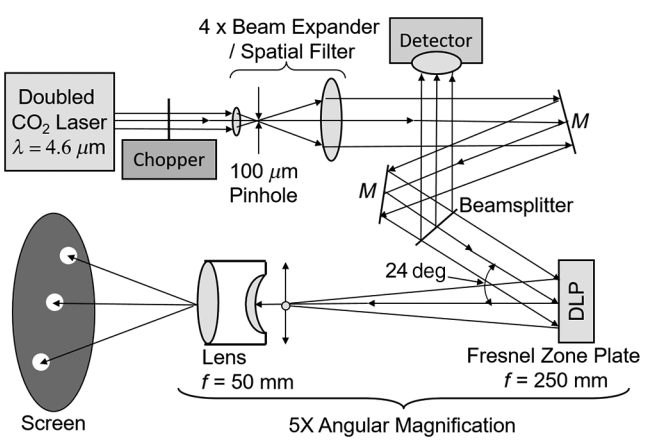

Fig. 1 Experimental setup.

2.1 *Laser*

The laser source is a DEOS (DeMaria ElectroOptics Systems Inc.) GEM-400CD RF-excited carbon dioxide laser operating quasi CW at 9.24 μm, and it is frequency double to obtain 1 W at 4.62 μm. An external acousto-optical modulator is used to control the intensity of the laser beam. The divergence of the laser was measured to be ∼4 mrad, the quoted specification was <4.5 mrad. The laser is linearly polarized along the horizontal direction.

2.2 *SLM*

The SLM is a Texas Instruments DLP7000 XGA DMD, commonly called the digital light projector, or DLP. The DLP format is 768×1024 micromirrors on a 13.68-μm pitch (10.5×14 mm). The mirrors rotate about a diagonal hinge and have two stable positions, $+12 \pm 1$ deg (binary 1) or -12 ± 1 deg (binary 0). The reflective surface of the mirrors is aluminum, and their reflectivity is ∼95% at 4.6 μm. Since TI does not specify the reflectivity of their device at 4.6 μm, the reflectivity is estimated from typical spectral curves supplied by an aluminum mirror supplier; such as Thorlabs. The fill factor is 91% at normal incidence; the mirrors are 13.05 μm^2 with a 0.63-μm gap between mirrors. The glass window was replaced with an uncoated calcium fluoride window (single pass transmission = 0.945) for IR operation. When a flat binary 1 pattern is rendered, the measured reflectivity of the device (reflection losses due to the window are removed because they are not an inherent property of the DLP) is ∼67% into the zeroth-order. The theoretical maximum efficiency η into the zeroth-order would be the square of the product of the mirror reflectivity and the fill factor; that is, $\eta = [0.95 * 0.91 * \cos(12)]^2 = 71.5\%$. Since the unprotected aluminum micromirrors were exposed to the atmosphere (TI hermetically seals the DLP) when the window was replaced, it is possible that the reflectivity is degraded a few percent, and the reflectivity could be as low as $92\{\eta = [0.92 * 0.91 * \cos(12)]^2 = 67\%\}$ in agreement with our measurement.

The DLP is a binary device and the reflectance of a binary amplitude grating rendered on the DLP is given as

$$r(x) = r_0[1 + \mathrm{SQ}(x)]/2, \tag{1}$$

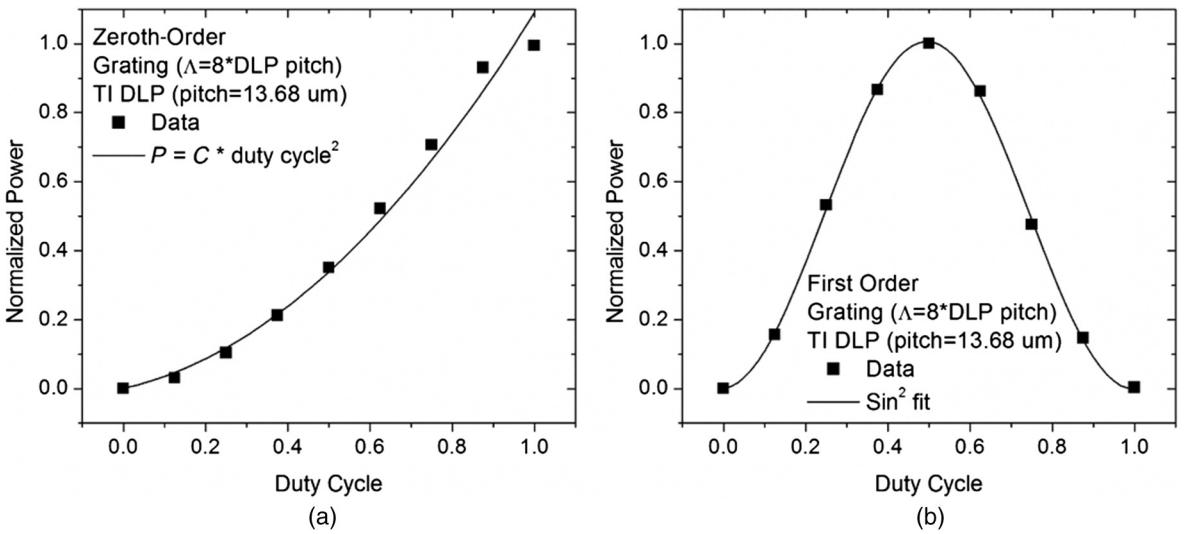

Fig. 2 (a) Normalized power in the zeroth-order as a function of spatial duty cycle of an 8 pixel period grating and (b) the normalized power in the first order as a function of spatial duty cycle. The lines drawn through the data are curve fits to the data.

where r_0 is the reflectivity of a micromirror and SQ is a square waveform with periodicity Λ. For a 50% spatial duty cycle, the square waveform is defined as

$$\mathrm{SQ}(x) = \begin{cases} -1 & \text{for } 0 \le x < \frac{\Lambda}{2} \\ 1 & \text{for } \frac{\Lambda}{2} \le x < \Lambda \end{cases}. \tag{2}$$

Thus, 50% of the light is reflected by the mirrors tilted at 12 degs (binary 1) and 50% of the light is reflected into a beam dump by the mirrors tilted to −12 deg (binary 0). Of the light reflected by the binary 1 mirrors, 50% will remain in the zeroth-order and the remainder is shared by the diffracted orders. The theoretical maximum diffraction efficiency of a binary amplitude diffraction grating with 50% spatial duty cycle is 25% (fill factor squared) into the zeroth-order and ∼10% [calculated by $(2 \text{ fill factor}/\pi)^2$] into the first-order.[18,19] The reflectivity of a binary grating is proportional to the area of the mirrors in the "on" state. The remainder of the light is diffracted into higher orders. With the added inefficiency of the mirrors tilted at 12 deg, the estimated maximum efficiency of the DLP into the first-order would be 8.6% $[(0.95\cos(12)/\pi)^2]$.

Although the DLP is a binary device, the intensity of the light reflected and diffracted can be controlled by several techniques. Dudley et al.[21] demonstrated that the intensity of the diffracted light could be modulated by varying the on-time and/or dithering the mirrors. The DLP can refresh at rates greater than 10 kHz; therefore, one could encode the laser beam with information. In addition, the intensity can be controlled by varying the spatial duty cycle of the diffraction pattern as shown in Fig. 2. Figure 2(a) is a plot of the normalized power in the zeroth-order as a function of duty cycle for a grating with a period of 8 pixels (e.g., a 25% spatial duty cycle grating is when 2 adjacent pixels are in the "on" state and 6 pixels are in the "off" state). The line drawn through the data illustrates that the zeroth-order efficiency depends on the square of the duty cycle. Figure 2(b) is the corresponding plot of the normalized power diffracted into the first-order. The first-order diffraction efficiency peaks at 50% spatial duty cycle. The line drawn through the data is a $\sin^2$ curve fit to the measured data.

In this paper, binary amplitude FZPs calculated for specific angles and wavelengths are rendered on the DLP rather than gratings, and it is expected that the efficiency of a binary amplitude FZP will approach the theoretical limit of 10.1% on-axis[19] and fall off with a $\sin^2$ dependence on the steering angle. Intensity control with the FZP is also demonstrated using the concepts developed in Fig. 2; that is, controlling the intensity by varying the fill factor of the binary amplitude diffraction pattern.

Texas Instruments conducted tests on the DLP and determined that the maximum operating temperature is 150°C[22] and that the CW optical damage threshold is 25 W/cm^2. However, this might be a conservative estimate, as several researchers have reported irradiating a single micromirror on the device with CW intensity levels exceeding 10,000 W/cm^2 without observing damage.[23,24] Assuming the conservative damage threshold reported by TI and the area of our device (1.47 cm^2), the device can conservatively handle 37 W without damage and active cooling of the DLP would extend the operating temperature range.

2.3 *Camera*

An FLIR SC4000 MWIR InSb camera (nominally 3 to 5 μm spectral response) is used to observe and profile the laser beam. The array format is 320×256 pixels on a 30-μm pitch. The camera lens is a Janos ASIO MWIR lens ($f/\# = 2.3$; $f = 25$ mm). The camera is necessary to locate the invisible beam steered across the screen in Fig. 1 when measuring the steering angle. In addition, the camera is used to record videos demonstrating beam steering. The lens is removed to profile the laser beam and measure its spot size. When the camera is used, the chopper is turned off in the open state.

2.4 *Recollimating Lens*

A Mitsubishi IR-L50B lens collimates the laser beam. Its focal length is 50 mm, and its $f/\#$ is 1.2. The field-of-view is ∼45 deg [FOV $= 2 * \mathrm{atan}(1/2 * f/\#)$]. The

transmission of the lens was measured to be 0.9375 at 4.6 μm.

2.5 *MWIR Detectors*

A pair of PbSe detectors (Thorlabs PDA20H) was used to simultaneously measure the incident and diffracted power. Because the detector size is small (2 mm × 2 mm), a 1-in.-diameter calcium fluoride lens focuses the light on the detector element. These detectors also require that the laser beam be modulated by an optical chopper (see Fig. 1). The output of each detector was fed into a lock-in amplifier (Stanford Research Systems SR530) and the output of both lock-in amplifiers was digitized. Calibrated filters were inserted into the beam to avoid saturating the lock-in amplifiers and detectors.

3 Results

The binary amplitude FZP is derived from a spherical wavefront whose field is given as

$$E = e^{i\pi\frac{(x-x_0)^2+(y-y_0)^2}{\lambda f}}, \tag{3}$$

where f is the focal length of the FZP, λ is the laser wavelength, and x_0 and y_0 are the coordinates of the zone center. A beam is steered by moving the zone center (x_0, y_0). The zone center can be randomly positioned at the frame rate, and its position is not constrained to the physical dimensions of the SLM. In an operational system, the azimuth and elevation can be determined independently and the corresponding values of x_0 and y_0 calculated. It should also be noted that the wavelength of light could be randomly chosen from a repertoire of available copropagating lasers. The phase of the field is calculated using the four-quadrant inverse tangent function where the argument is the ratio of the imaginary and real parts of the field. The amplitude of the phase is computed, the results normalized, and then converted to binary before rendering the binary pattern on the DLP. If the mirror value is greater than 0.5, it is assigned a value of 1 (+12 deg tilt), otherwise it is assigned a value 0 (−12 deg tilt).

Figure 3 is a plot of the power as a function steering angle θ of the FZP-only (no recollimating lens) measurement, and the solid line is a $\sin^2(\theta)$ fit to the data. Note that there is no data point at 0 deg due to the presence of the zeroth-order, which dominates the signal and cannot be discriminated against or removed without the recollimating lens. In addition, the shift in the curve to the positive angles is the result of the DLP alignment procedure. A HeNe alignment laser is backreflected from the DLP when the device is floating with no applied voltage. Although the floating mirror orientation was reproducible, the floating mirror orientation is not a controlled position (not a tristate device). Consequently, the bisector to the binary 0 (-12 ± 1 deg) and binary 1 ($+12 \pm 1$ deg) mirror orientations are not symmetric about the floating mirror normal and thus, the floating mirror normal does not coincide with the grating normal.

Figure 4 is a plot of the power as a function of steering angle with the recollimating lens forming a 5× telescope. In this case, the recollimating lens collimates the light focused by the FZP but focuses the light in the zeroth-order causing it to diverge rapidly in free space as it propagates to the screen. Consequently, the light in the zeroth-order has minimal contribution to the on-axis intensity at distances long compared

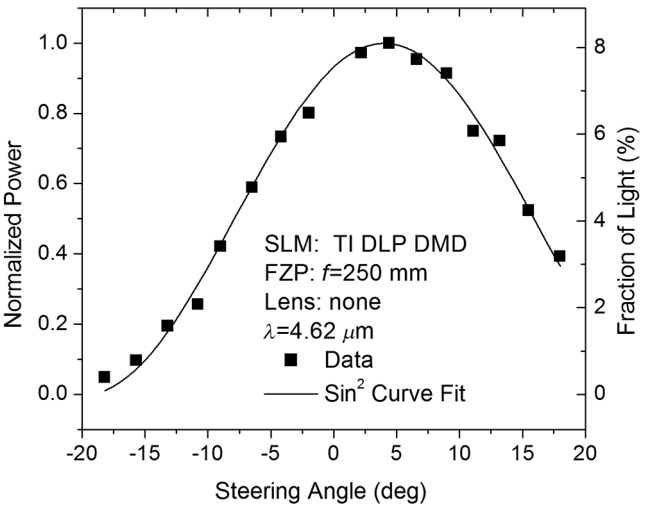

Fig. 3 Normalized power in the steered beam as a function of steering angle with no recollimating lens. The on-axis data point is not plotted due to the presence of the zeroth-order.

to the focal length of the recollimating lens. The zeroth-order could be suppressed,[25] but it is not necessary for our application. Again, the solid line through the data is a $\sin^2(\theta)$ fit to the data, and the curve is shifted as in Fig. 3. The measured steering range is 42 deg (−21.6 to 20.8 deg) and is consistent with the FOV of the recollimating lens. The aperture of the recollimating lens and the magnification of the telescope limit the maximum angle in Fig. 4. A customized lens would produce a larger steering range. The data points in Fig. 4 correspond to the data near 0 deg in Fig. 3 (between −4 deg and 4 deg) where the data are rapidly changing. However, due to the small angular range, the power varies by less than 25% in Fig. 4. Figure 5 is a recording of a beam being steered across the field of engagement. A lens with a smaller $f/\#$ would produce a larger steering range although the power variation would be greater; that is, it will follow the $\sin^2(\theta)$ dependence as shown in Fig. 3.

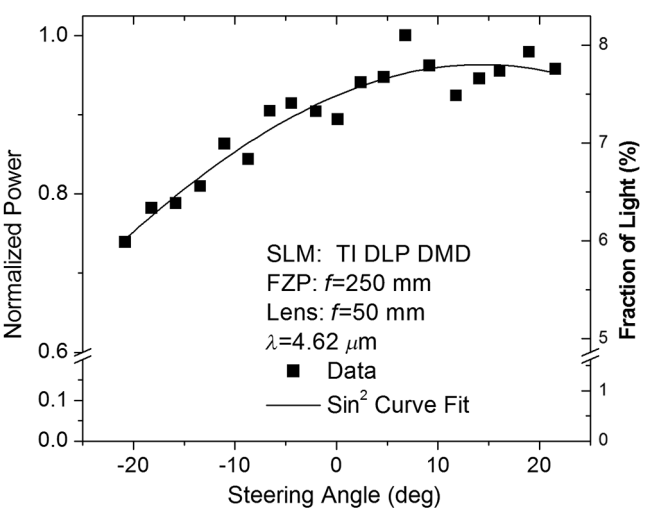

Fig. 4 Normalized power in the recollimated steered beam as a function of steering angle. The maximum angle is limited by the field-of-view of the recollimating lens. Beam steering is demonstrated in Fig. 5.

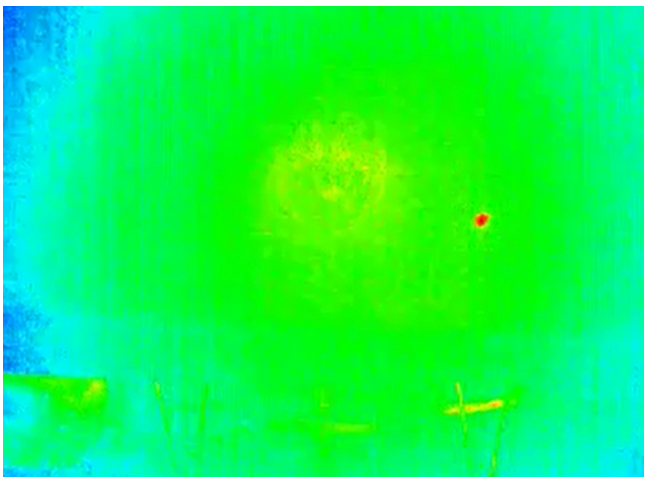

Fig. 5 Recording of a beam steered in a line across the field of engagement. A delay of 300 ms is inserted between each movement to ensure that the free-running camera captures every movement. (Video 1, mp4, 1.1 MB [URL: https://doi.org/10.1117/1.OE.57.2.027108.1].)

The diffraction efficiency, measured on-axis, is 8.1% and follows a $\sin^2(\theta)$ dependence on angle as shown in Fig. 3. If a 37-W beam is incident on the SLM, then there would be over 3 W steered on a target that is on-axis.

The divergence of the steered beam was measured by directly observing the beam with a MWIR thermal imager with the lens removed. The profile of the collimated beam is Gaussian and the spot size was measured at two positions, separated by 576 mm. The spot sizes were determined from Gaussian fits to the measured profiles at both positions. The results are shown in Fig. 6. The divergence was calculated to be 5.2 mrad and is consistent with the magnification of the optical system and the divergence specified by the laser manufacturer, DEOS.

Figure 7 demonstrates intensity control of the steered beam using a binary amplitude SLM. Intensity control is implemented by varying the binary amplitude threshold level, which determines the number of mirrors in the binary 1 state. As expected, the peak intensity corresponds to a 50% spatial duty cycle. The line drawn through the data is a $\sin^2$ curve fit to the measured data.

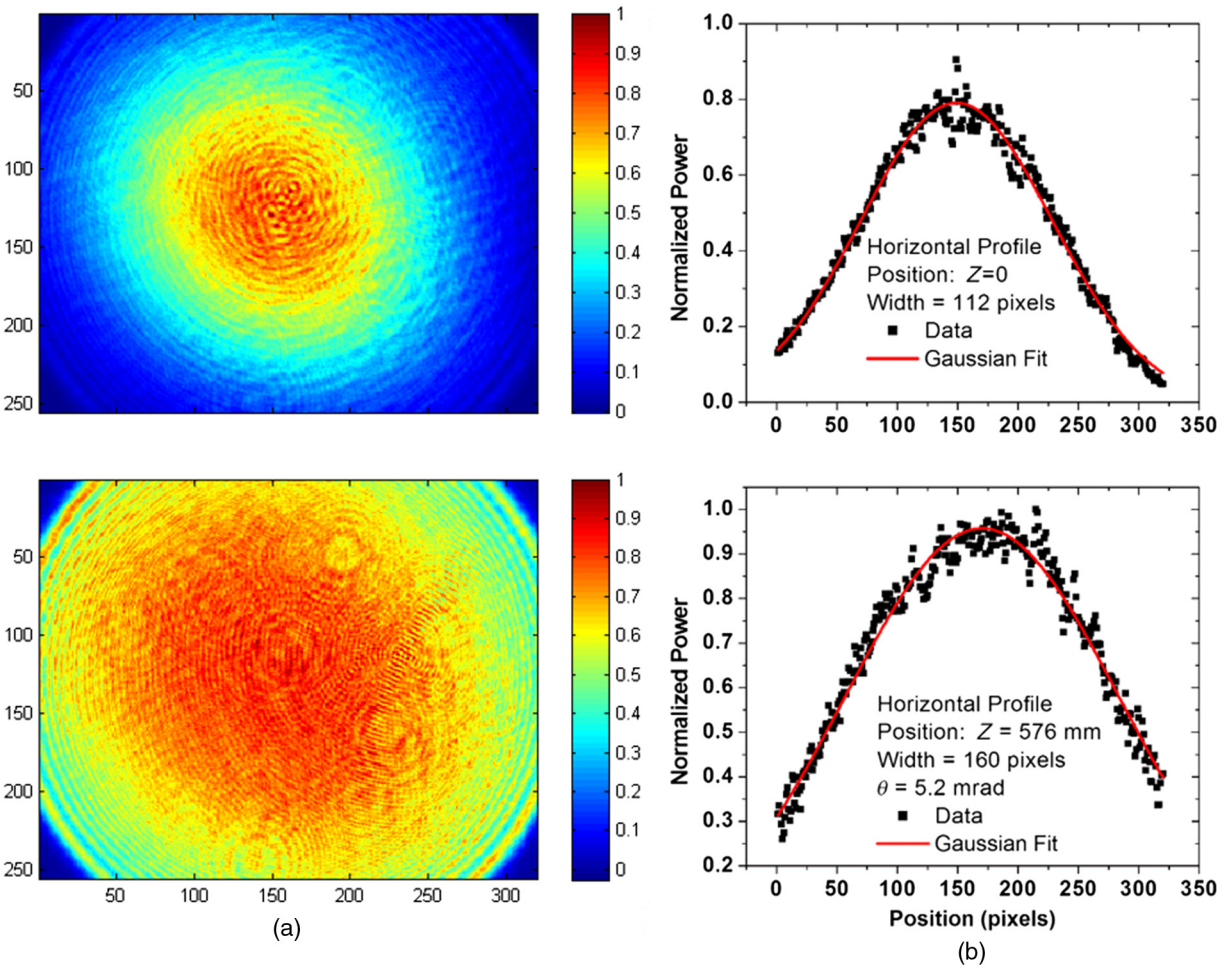

Fig. 6 Profile of the steered laser beam measured at two positions along the propagation of the beam. (a) Images of the laser beam at the two positions and (b) the corresponding line profile of the laser beam. The distance between the two positions is 576 mm. The line drawn through the data points is a Gaussian curve fit. The measured divergence is 5.2 mrad.

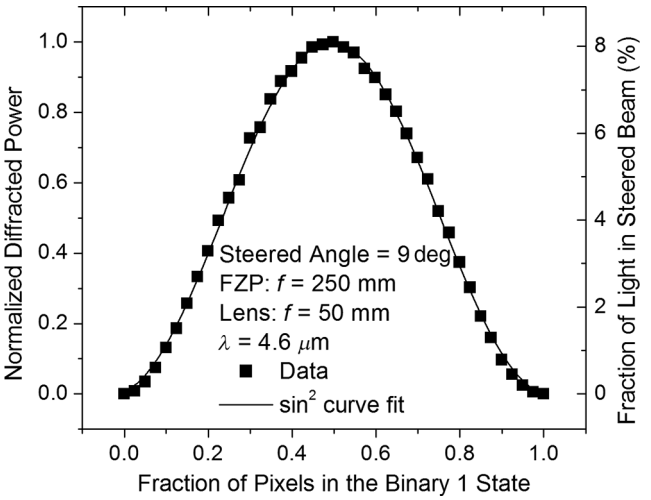

Fig. 7 Normalized power diffracted into a beam steered at 9 deg as a function of the percent of pixels in the binary 1 state. The line through the data is a $\sin^2$ curve fit to the data. Intensity control is demonstrated in Fig. 8.

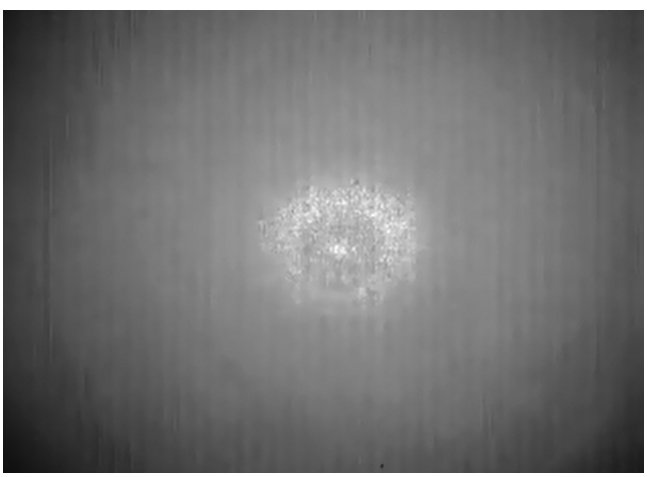

Fig. 8 Recording demonstrating intensity control (Video 2, mp4, 647 KB [URL: https://doi.org/10.1117/1.OE.57.2.027108.2].)

An advantage of the holographic beam steering technique is that multiple beams can be derived from a single hologram by superimposing computer-generated fields calculated from Eq. (3) for a specific wavelength and position. The composite field F is given by

$$F(x_0, y_0, \lambda) = \frac{w_1 * E_1 + w_2 * E_2 + \ldots.. + w_n * E_n}{\sum_1^n w_i}, \qquad (4)$$

where the w_j's are weighting coefficients that control the relative strength of the n fields, $E_n(x_0, y_0, \lambda)$. The phase of the field is calculated as before from the four-quadrant inverse tangent function. The amplitude of the phase is computed, normalized, converted to binary, and imprinted on the DLP.

Two FZP were calculated [Eq. (3)] and superimposed [Eq. (4)] to generate two laser beams. One beam was steered to 9 deg $[(x_0, y_0) = (400{,}400)]$ and the other was steered to -9 deg $[(x_0, y_0) = (-400, -400)]$, a dual-symmetric composite FZP. The power was measured in each beam,

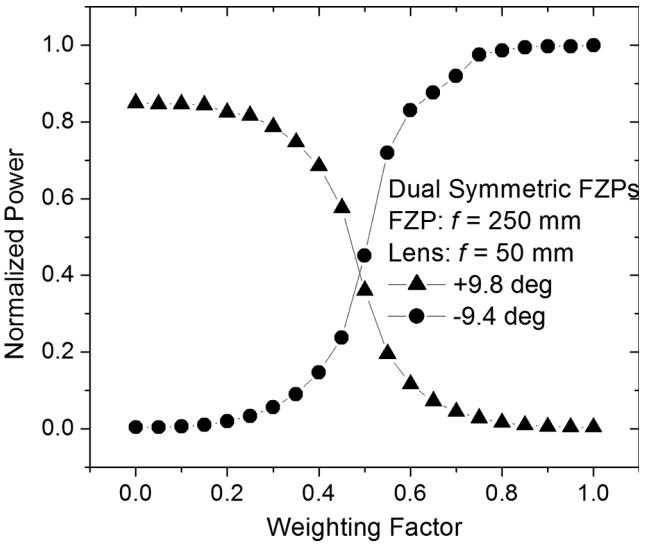

Fig. 9 Normalized power in each beam for a dual symmetric composite FZP as a function of the relative weighting factor. As the relative weighting factor is varied, the power is transferred from one beam to the other. See Video 3. The power asymmetry is due to alignment. This asymmetry is also seen in Figs. 3 and 4 and its origin is discussed above.

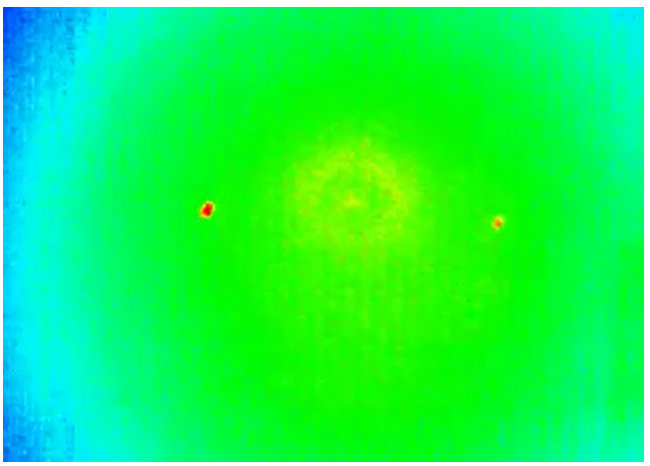

Fig. 10 Video recording of energy transfer from one beam to the other from a dual composite FZP rendered on the SLM. (Video 3, mp4, 1.8 MB [URL: https://doi.org/10.1117/1.OE.57.2.027108.3].)

and the results were compared to the corresponding single FZP steered to ± 9 deg, respectively. Approximately 44% of the light was in each of the beams revealing that 12% of the light is lost, scattered into unwanted directions due to field crossterms. Figure 9 is a plot of power measured for each beam as a function of weighting factor as the power is transferred from one beam to the other in a dual off-axis FZP. Figure 10 demonstrates this transfer of power from one beam to the other.

Multibeam beam steering is demonstrated in Fig. 11. Four beams are generated and steered off-axis with one being steered in a circle. The video also illustrates that each beam can be independently steered and that they are randomly addressable. The number of beams created by superimposing FZPs is only limited by the laser power required to accomplish the task at hand.

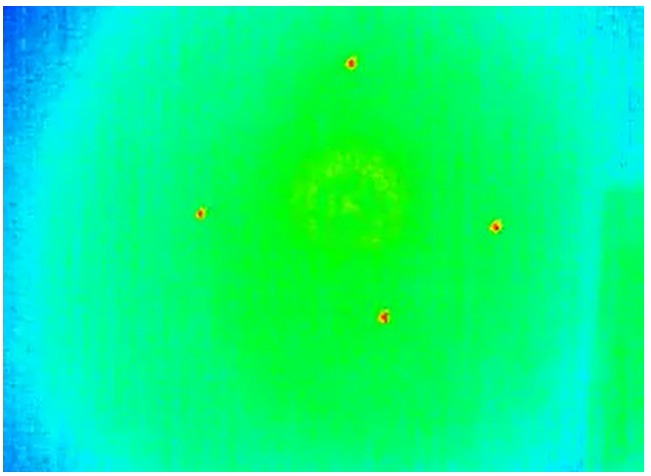

Fig. 11 Video recording of multiple beams steered simultaneously across the field of engagement. A delay of 300 ms is inserted between each movement to ensure that the free-running camera captures every movement. (Video 4, mp4, 1.0 MB [URL: https://doi.org/10.1117/1.OE.57.2.027108.4].)

4 Conclusions

Large angle, nonmechanical beam steering is demonstrated at 4.62 μm using the DLP technology. A 42-deg steering range is demonstrated, limited by the FOV of the recollimating lens. The measured diffraction efficiency is 8.1% on-axis and falls-off with a $\sin^2(\theta)$ dependence on the steering angle. Moreover, the power varied less than 25% within the 42 deg steering range. The profile of the laser is Gaussian with a divergence of 5.2 mrad. The ability to control the intensity of the steered beam is also demonstrated. Furthermore, multibeam, randomly addressable, beam steering is demonstrated. Finally, the knowledge gleaned from previous research using a phase-only SLM applies almost seamlessly to the binary amplitude device at MWIR wavelengths.

While the efficiency of the DLP is low, the damage threshold is sufficiently high to steer a high intensity laser beam on target. Thus, the DLP technology is a viable solution to nonmechanical beam steering in the MWIR spectral region. In addition, the performance of the DLP would improve if it were optimized for MWIR operation. Next, we plan to use a high power QCL laser (Forward Photonics, LLC and TeraDiode, Inc.) to demonstrate agile wavelength beam steering in the MWIR spectral region. The laser consists of 13 copropagating lasers with central wavelengths spanning nearly 200 nm. Previous results[13] in the visible spectral region indicate that the output of each or all of the individual lasers diodes can be steered on target either simultaneously or sequentially.

References

1. M. Zorabi, R. H. Cormack, and J. T. Gopinath, "Wide-angle nonmechanical beam steering using liquid lenses," *Opt. Express* **24**(21), 23798–23809 (2016).
2. M. A. Powers and C. C. Davis, "Spectral LADAR: towards active 3D multispectral imaging," *Proc. SPIE* **7684**, 768409 (2010).
3. H. D. Tholl, "Novel laser beam steering techniques," *Proc. SPIE* **6397**, 639708 (2006).
4. M. J. R. Heck, "Highly integrated optical phased arrays: photonics integrated circuits for optical beam shaping and beam steering," *Nanophotonics* **6**(1), 93–107 (2017).
5. M. Ziemkiewicz et al., "Laser-based satellite communication systems stabilized by non-mechanical electro-optic scanners," *Proc. SPIE* **9828**, 982808 (2016).
6. X. Wang et al., "Modeling and design of an optimized liquid-crystal optical phased array," *J. Appl. Phys.* **98**, 073101 (2005).
7. J. R. Lindle, A. T. Watnik, and V. A. Cassella, "Efficient, multi-beam large angle, non-mechanical, laser beam steering from computer-generated holograms rendered on a liquid crystal spatial light modulator," *Appl. Opt.* **55**(16), 4336–4341 (2016).
8. J. Sun et al., "Large-scale nanophotonic phased array," *Nature* **493**, 195–199 (2013).
9. J. Kim et al., "Wide-angle, nonmechanical beam steering with high throughput utilizing polarization gratings," *Appl. Opt.* **50**(17), 2636–2639 (2011).
10. S. R. Davis et al., "Analog, non-mechanical beam steerer with 80 degrees field of regard," *Proc. SPIE* **6971**, 69710G (2008).
11. T. E. Dillon et al., "Nonmechanical beam steering using optical phased arrays," *Proc. SPIE* **8184**, 81840F (2011).
12. C. Florea, J. Sanghera, and I. Aggarwal, "Broadband beam steering using chalcogenide-based Risley prisms," *Opt. Eng.* **50**(3), 033001 (2011).
13. J. R. Lindle, A. T. Watnik, and V. A. Cassella, "Wavelength agile nonmechanical laser beam steering from Fresnel zone plates imprinted on a liquid crystal spatial light modulator," *Opt. Eng.* **55**(9), 097103 (2016).
14. J. A. Frantz et al., "Non-mechanical beam steering in the mid-wave infrared," *Proc. SPIE* **10181**, 101810X (2017).
15. S. T. Wu, "Infrared properties of nematic liquid crystals: an overview," *Opt. Eng.* **26**(2), 262120 (1987).
16. W. Duncan et al., "DLP switched blazé grating: the heart of optical signal processing," *Proc. SPIE* **4983**, 297–304 (2003).
17. H. H. Refai, J. J. Sluss, and M. P. Tull, "Digital micromirror device for optical scanning applications," *Opt. Eng.* **46**(8), 085401 (2007).
18. P. A. Blanche et al., "Diffraction-based optical switching with MEMS," *Appl. Sci.* **7**(4), 411–421 (2017).
19. Q. Cao and J. Jahns, "Comprehensive focusing analysis of various Fresnel zone plates," *J. Opt. Soc. Am. A* **21**(4), 561–571 (2004).
20. C. M. Titus et al., "Diffraction efficiency of thin film holographic beam steering devices," *Proc. SPIE* **4825**, 177–188 (2002).
21. D. Dudley, W. Duncan, and J. Slaughter, "Emerging digital micromirror device (DMD) applications," *Proc. SPIE* **4985**, 14–25 (2003).
22. Texas Instruments, "Laser power handling for DMDs," *DLPA027 Datasheet* (2012), http://www.ti.com/lit/wp/dlpa027/dlpa027.pdf.
23. A. R. Faustov, M. R. Webb, and D. R. Walt, "Note: toward multiple addressable optical trapping," *Rev. Sci. Instrum.* **81**(2), 026109 (2010).
24. B. Schwartz et al., "Laser-induced damage threshold of camera sensors and micro-optoelectromechanical systems," *Opt. Eng.* **56**(3), 034108 (2017).
25. S. Y. Wu, J. Liang, and M. F. Becker, "Suppression of the zero-order diffraction beam from computer generated holograms produced by a DLP spatial light modulator," *Proc. SPIE* **8254**, 82540C (2012).

James Ryan Lindle is a research physicist at NRL. He has authored over 100 papers, including papers on nonmechanical beam steering, midwave infrared laser development, negative luminescence, nonlinear optical properties of materials, optical limiters, electronic properties of semiconductors, electro-optical properties of liquid crystals, and susceptibility of focal plane arrays to laser countermeasures. He holds patents on laser hardening of detectors, optical limiters, and MWIR lasers. Three of his laser patents are currently licensed.

Abbie T. Watnik is a research physicist at US Naval Research Laboratory in the Optical Sciences Division. She received her BS degree in electrical engineering from Colorado State University and her MS and PhD degrees in optics from the University of Rochester. Her current research interests include optical phase conjugation, nonmechanical holographic beam steering, computational imaging approaches, and optical vortices for imaging applications. She is a member of SPIE.